Advances in Science and Technology Research Journal

Advances in Science and Technology Research Journal 2023, 17(6), 378–387
https://doi.org/10.12913/22998624/175142
ISSN 2299-8624, License CC-BY 4.0

Received: 2023.10.23
Accepted: 2023.11.10
Published: 2023.11.23

Computational and Experimental Investigation of Inert Gas Flow Field in Direct Metal Laser Melting Printer Build Chamber

Paweł Czekałowski[1*], Wit Stryczniewicz[2], Paweł Żuk[1], Krzysztof Panna[2], Paweł Borkowski[2], Michał Bujak[1], Tomasz Iglewski[1]

[1] General Electric Aerospace Poland Sp. z o.o. Al. Krakowska 110/114 02-256 Warszawa, Poland
[2] Łukasiewicz Research Network – Institute of Aviation, Al. Krakowska 110/114 02-256 Warszawa, Poland
* Corresponding author's e-mail: pawel.czekalowski1@ge.com

ABSTRACT

Additive manufacturing methods are becoming more and more popular in today's production market. These methods became a useful and flexible alternative to traditional manufacturing approach. One of the most popular methods in this family is direct metal laser melting. It can achieve high quality prints, however, numerous parameters need to be established, to achieve a good quality product. One of the aspects of printing process is inert gas flow. The goal of presented study is to quantitatively assess inert gas flow field using both experimental and numerical methods. Flow field parameters have been measured with anemometry and particle image velocimetry (PIV). Additionally computational fluid dynamics (CFD) tools were used to investigate flow phenomena occurring inside the build chamber. PIV measurements give good insight into the flow field, but they are costly and require significant time for preparation. For this reason, CFD analysis is widely used as a design tool, giving reasonable turnaround time. In addition, every design tool to be reliable need to be validated against test data. In this study the team was able to collect both experimental and numerical data and finally conduct the validation. Work allowed to determine the most suitable approach for predictions in given problem. Different turbulence models have been tested. Simulation results were validated against collected experimental data.

Keywords: additive manufacturing, inert gas flow, particle image velocimetry, computational fluid dynamics

INTRODUCTION

Quality of additively manufactured parts depends on numerous parameters. Laser power settings and control, scanning strategy or speed are the most basic variables, that impact print result [1, 2]. Inert gas flow is not obvious factor, however wrong settings can have a significant impact on many characteristics of the mechanical properties, part conditions and process stability, such as, for example: surface roughness [3], porosity [4, 5], homogeneity [6], and keeping the powder bed and the area between the laser source and the print surface as clean as possible to avoid any laser beam disruptions [7, 8].

To maintain the appropriate high stability, repeatability, speed, quality, and purity of the additive process in the laser powder bed fusion technology, it is necessary to ensure a good discharge of by-products from the melting process. For this purpose, to effectively get rid of by-products such as spatter or soot from above the surface of the powder bed, an efficient gas flow over the build plate is necessary [20]. Currently a key machine providers like GE Additive focuses on the evolution of the gas flow during continuous improvement efforts on direct metal laser melting (DMLM) machines and how the associated build process was improved due to in-depth research into the underlying physics of the melting process [9].

Inert gas flow nowadays is a field of extensive exploration. Several papers on computational modelling of inert gas flow have been published recently. Philo et al. [10, 11] used computational fluid dynamics (CFD) modelling to investigate inlet system design of DMLM machine. Yu Chen

et al. [12] tried to optimize flow inside chamber of the same printer type. Gas flow field is analyzed also with experimental methods [13, 14]. Schniedenharn et al. [15] developed space-resolved thermal anemometry to investigate flow inside commercial L-PBF machine. Chen et al. [16] used both numerical and experimental approaches to investigate flow in chamber using so called push-pull flow system. Gas flow phenomena need to be considered also in spatter behavior analysis. Chien et al. [17] have analyzed experimentally and numerically spattering phenomena in the printer. Team used CFD coupled with discrete element method (DEM) to model particles trajectory. Predictions were compared to the trajectories recorded with Camera in printer.

Open literature study show, that investigation of inert gas flow inside printer chamber is a modern topic. Most of experimental methods use anemometry technique, that delivers medium velocities in discrete locations. Current study is based on PIV measurements, that deliver view of entire flow field. Not many examples of PIV measurements in 3D printer chamber can be found. An example can be found in study experiment performed by Chen et al. [18], however test was performed on system with significantly different flow field architecture.

Computational fluid dynamics is analytical method widely used in variety of applications. Utilization of such analyses can be found in aviation, automotive, health care and many other branches of industry. Researchers and engineers reach for CFD very often once insight in complicated flow structure is desired. Although CFD is very universal and powerful tool, it has some deficiencies and imperfections. There are many approaches and strategies to conduct CFD analysis, that may lead to different (more or less accurate) result. The key for reliable design tool is to know how well analysis reflects reality. To gather this knowledge analysis results, need to be compared against test data. Goal of this study is to prepare reliable and useful design tool for analysis inert gas flow features of DMLM machines. In the other hand the study proves usefulness of PIV measurements in DMLM printer design process.

EXPERIMENTAL STUDY

Printer inert gas flow demonstrator

DMLM printer chamber has visual access enabling visual inspection during printing, but it is insufficient to perform PIV measurements. To gather detailed flow field measurements, it has been decided to build demonstrator, that will reflect printer chamber and mimic inert gas flow field. Demonstrator vessel (without PIV system) is shown in Figure 1. Test stand has been designed enabling visual access for laser sheet and PIV system camera. Great care has been taken to reproduce real machine flow field. Demonstrator has been equipped with inlet and conditioning section, that mimics original hardware. Inert gas flow demonstrator was supplied with air from controlled supply system and spent gas into atmosphere. Flow field has been validated with anemometry using machine flow calibration procedure. The printer uses nitrogen as an inert gas flow, but due to test simplification air was used in

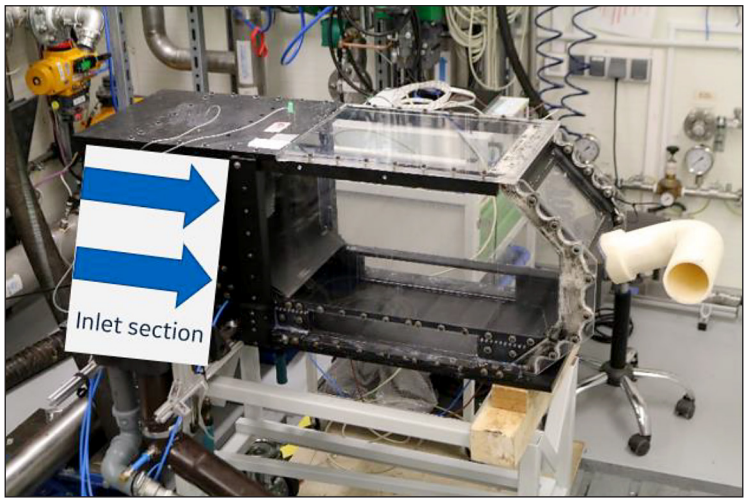

Figure 1. Inert gas flow demonstrator

PIV test instead. Air mass flow rates have been scaled to satisfy Reynolds number similarity. 2D PIV measurements have been performed on 12 vertical planes parallel to main printer flow. Measurement plane change was realized by manual adjustment of demonstrator position in camera axis direction. Rest of the measurement system was left untouched, so there was no need PIV system recalibration.

PIV method

PIV technique has been used for volumetric measurements of 3D flows for over two decades, starting from multiple plane stereo particle image velocimetry [19] to investigations of instantaneous 3D flow fields CA [20]. Recently, 2D PIV technique has been successfully applied for investigation of complex 3D flow field generated by multirotor [22, 23].

PIV measurements was performed on dedicated test stand. Main test idea and its realisation is shown in Figure 2. 2D2C PIV system consisted of three 4 MP cameras with 50 mm lenses and dual-cavity solid-state (Nd:YAG) pulse laser (330 mJ @ 532 nm). To visualize the flow in the main chamber two Dantec HiSense 620 cameras was used. The cameras were mounted side-by-side in such a way that the common Field of View included the whole area of the main chamber. The FOV of Camera #1 included the flow closer to the gas inlet and FOV of Camera #2 included the flow closer to the gas outlet. To investigate the flow over the bottom plate of the chamber Dantec SpeedSense VEO 640 camera was placed below Cameras #1 and #2. The FOV of Camera #3 included the flow directly above the bottom plate in such a way that the optical axis of the lenses was in line with the chamber bottom surface. The air was seeded with DEHS oil droplets generated by use of high output seeding generator with Lasikin nozzle system [23]. The nominal size of droplets was 2 μm. To provide uniform seeding density within the whole volume of the flow the seeding was introduced to settling chamber located downstream the main chamber of the printer. The Stokes number calculated for the investigated flow parameters was below 0.1 both for flow in the main chamber and over the bottom plate, assuring that the particles faithfully follow the flow [24]. The magnification of the lenses and the distance between the cameras and light sheet was set is such a way the particle images was above 2 pixels to avoid Peak Locking effect [24]. The particle images was processed using adaptive PIV interrogation scheme [25]. A series of 100 instantaneous velocity fields from each measuring plane was averaged to capture average flow filed. The cameras were placed in the distance of 500 mm from the light sheet. The light sheet was generated by light guided arm as in Figure 2.

Test results

PIV measurements delivered 2D flow field visualization in planes parallel to main direction of flow. To build quasi 3D view measurements have been repeated in 12 parallel planes. Measurement system was assembled with 2 cameras observing 2 sectors of demonstrator.

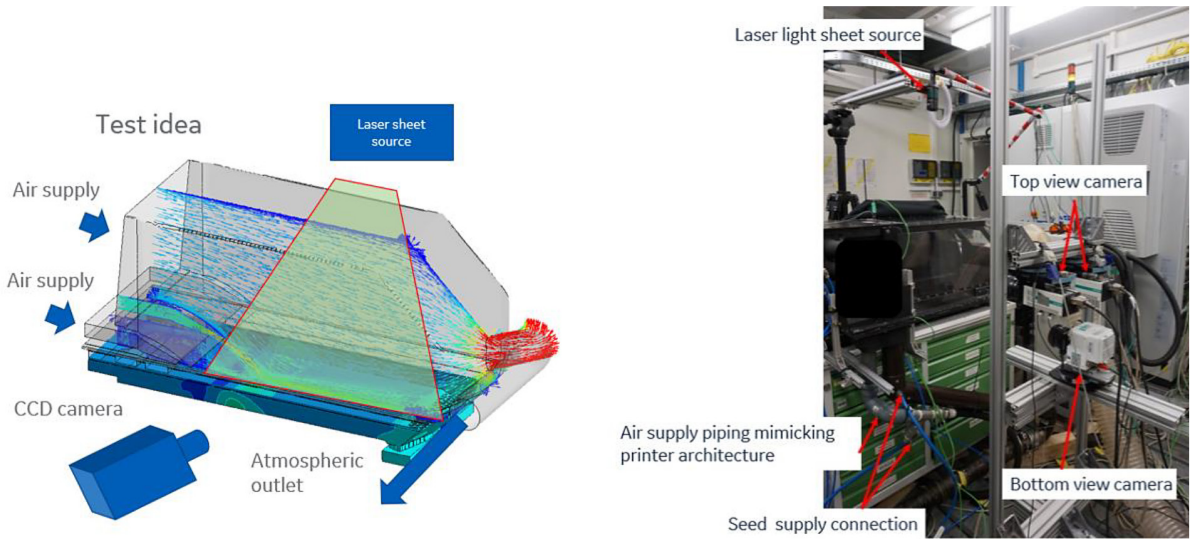

Figure 2. PIV test overview

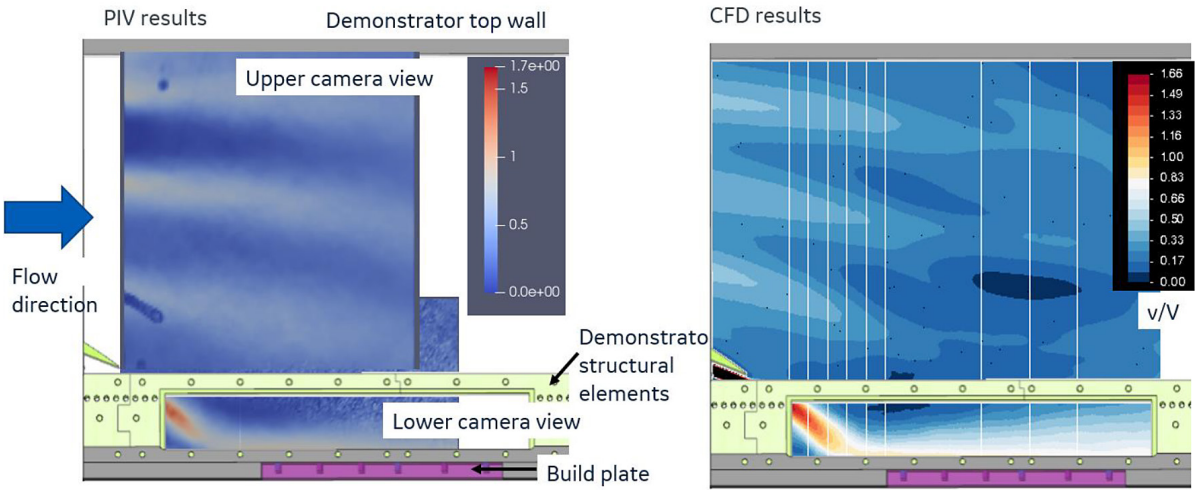

Figure 3. Single plane PIV measurements

One camera was focused on bottom flow which goes in direct vicinity of build plate. Second camera covered upper flow of demonstrator. The Figure 3. shows sample of single plane measurements collected on center plane. Picture contains views from two cameras. Additional side view sketch of demonstrator helps in understanding of image position. Sketch denotes position of build plate and shows location covered by demonstrator structure.

PIV measurements revealed two sectors of different velocity field, that is visible on center plane shown in Figure 3. Flow field near bottom wall is dominated with strong jet coming out from nozzle, travelling downward and reaches floor upstream of build plate. Jet after reaching impingement point travels in vicinity of wall towards outlet gradually dissipating. Rest of build chamber is flushed with air traveling with lower velocity. Flow visualization shows flow field structure with non-uniformities.

ANALYTICAL STUDY

Methods

Computational Fluid Dynamics nowadays is widely used numerical method for fluid mechanics analysis, very often used in complex problems in the automotive and aviation industries [26]. CFD solves Navier-Stokes equations with discrete methods. In this study calculations have been performed using commercial Ansys Fluent v19.4 package. Software solves continuity and momentum equations in form:

$$\frac{\partial \rho}{\partial t} + \nabla \cdot (\rho \vec{v}) = S_m$$

$$\frac{\partial}{\partial t}(\rho \vec{v}) + \nabla \cdot (\rho \vec{v} \vec{v}) = -\nabla p + \nabla \cdot (\bar{\bar{\tau}}) + \rho \vec{g} + \vec{F}$$

where:

$\bar{\bar{\tau}} = \mu \left[(\nabla \vec{v} + \nabla \vec{v}^T) - \frac{2}{3} \nabla \cdot \vec{v} I \right]$ – stress tensor,

ρ – density,
v – velocity,
t – time,
S_m – mass source,
p – pressure,
g – gravity acceleration,
F – force.

on domain divided with finite volumes. In the first line is continuity equation, second momentum equation. Wider description of finite volume method can be found in [27].

Analytical model reflects real machine geometry. Model consists of two main subdomains. First reflects entire inlet piping and conditioning section. Purpose of this part of the model is to ensure correct flow structure supplying build chamber. Second sub-domain that, is shown in Figure 4, represents printer build chamber. Model is equipped with two inlets, on which desired mass flow rate was enforced. Both bottom and upper flows are delivered through honeycombs. Lower honeycomb has been replicated with mesh, while upper represented with porous zone with anisotropic properties (to permit flow in one direction only). Hydraulic resistance has been adjusted to be the same as honeycomb replicated with the mesh. Domain has single

common outlet with constant (atmospheric) pressure boundary condition imposed.

Domain has been divided in ~82e6 polyhedral cells with 5 prismatic layers at wall boundary conditions. Due to expected higher velocity near bottom mesh in this region has been refined. Air at atmospheric conditions has been modelled with NIST real gas model built-in Fluent library. Three different turbulence models have been tested in this study. The least costly steady state RANS k-w SST model was used in first attempt. Later RANS Reynolds Stress Model has been checked. Finally, most expensive unsteady Stress Blended Eddy Simulation [28] using Dynamic Smagorinski turbulence model in LES region and k- w SST in RANS regions has been validated. In Table 1 main solver settings are listed. Calculations has been performed on cluster of 720 CPU (48 nodes) equipped 2880GB RAM memory.

Calculations results and validation

First quantitative CFD predictions validation can be done on contour plots comparison. In Figure 3 PIV image (left) with CFD contour plot (right) generated with approach 3 (approach with SBES turbulence model) have been compiled. Images show that, CFD model replicated all aerodynamic features in velocity field observed in demonstrator. On the bottom high velocity jet is present, that goes downwards and impinge floor and then creates film downstream. In the upper portion of view discrete jets coming from inlet sections are visible on both pictures. In Figure 5 velocity magnitude contour plots from all three approaches has been shown. It is visible that, on all three pictures the same features are visible, so quantitatively calculations provided similar results. Couple differences are worth noting. First is shape of lower flow jet and its dissipation. k-w SST model shows maximum jet velocity (in throat) exceeding 1.66v/V. this effect is caused by much thicker boundary layer predicted by k-w SST model comparing to others. Also, air velocity in film (downstream of impingement point) is higher 1.16 v/V vs 1.0 v/V. Second, shape of low velocity zone located near lower flow jet touchdown. RSM and SBES shows this zone bigger than k-w approach. Thirdly, upper flow jest dissipates slower in k-w model, than other two. To conduct quantitative comparison between CFD predictions and PIV measurements velocity profiles have been plotted along several control lines positioned perpendicular to flow main direction. Figure 6 shows comparison of normalized velocity profiles along 4 subsequent lines. Line L1 is

Table 1. Modeling approaches

Specification	Method 1	Method 2	Method 3
Turbulence model	k-ω SST	Reynolds stress (RSM)	SBES dynamic Smagorinsky with k-ω SST
Pressure-velocity coupling	SIMPLE	SIMPLE	SIMPLE
Gradient discretization	Least squares cell based	Least squares cell based	Least squares cell based
Pressure discretization	Second order	Second order	Second order
Momentum discretization	Bounded central differencing	Bounded central differencing	Bounded central differencing
Time discretization	Steady state	Steady state	Bounded second order implicit
Time step	N/A	N/A	2e-4s

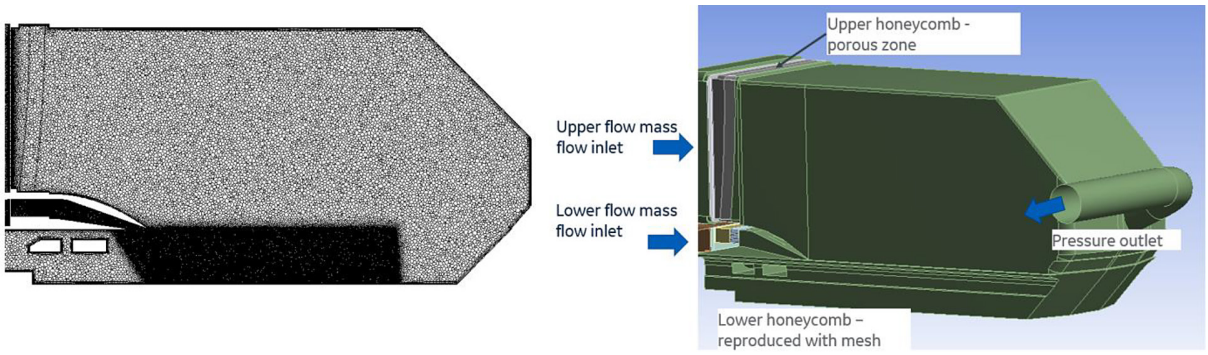

Figure 4. CFD domain and mesh

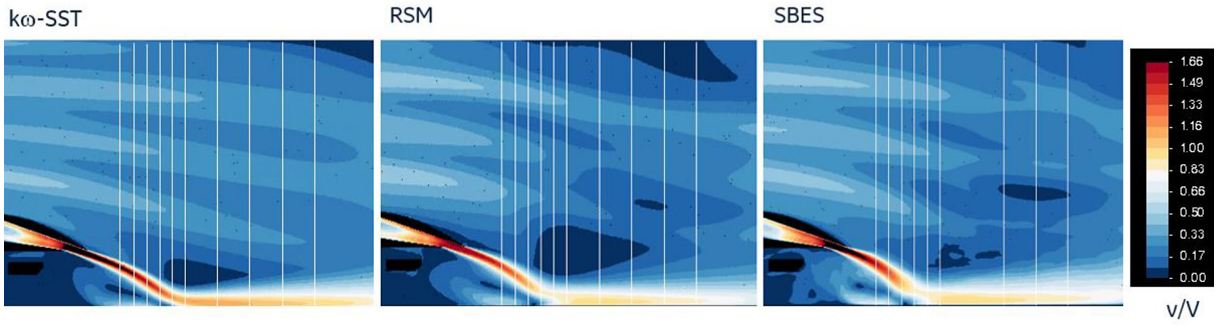

Figure 5. Normalized velocity magnitude in center plane

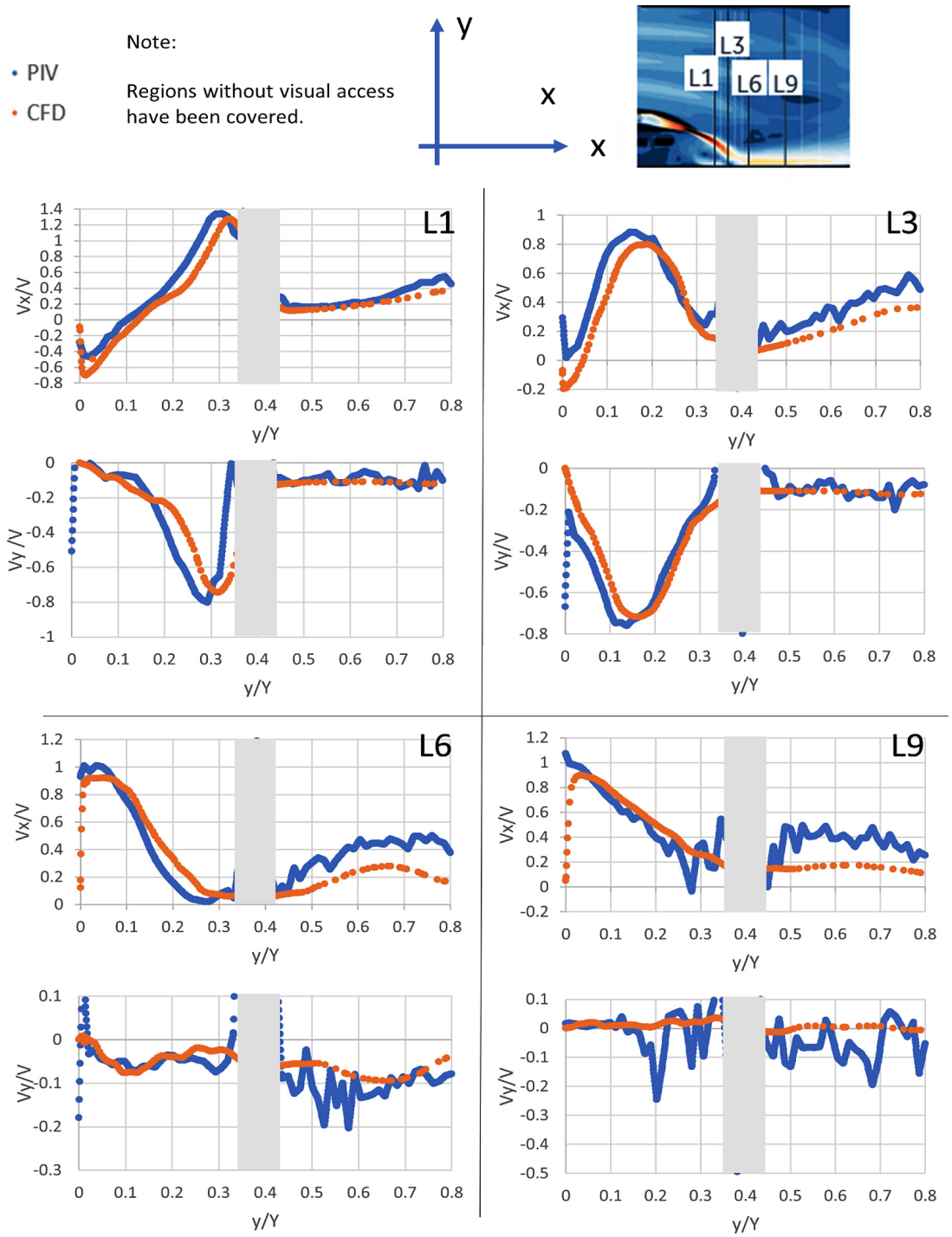

Figure 6. Normalized velocity profile evolution

the most upstream position visible for the camera, while L6 denotes edge of build plate. Vx/V and Vy/V are respectively horizontal and vertical flow velocity components normalized with reference velocity. y/Y is distance from bottom wall normalized with camera view height. Velocity peak on the plots represents jet coming from lower flow supply. Peak position gradually decreases reaching floor on line 6. Figure 6. Contains comparison of PIV measurements and CFD using SBES k-w turbulence model. CFD SBES k-w model replicated qualitatively and quantitatively well lower flow jet. Model shows jet in similar position and similar velocity in peak. Difference in Vx and Vy velocities are below ~10%. Position of peak differs with 0.01-0.037 y/Y. CFD plots follows the same trends at higher distances from the bottom wall, however differences are more distinctive.

Velocity profiles on lines 1-9 for RANS based methods qualitatively is not worse than SBES predictions except line 3. This has been illustrated in Figure 7. Velocity profiles on line L3 have been compared. Comparison shows that, RANS based approaches predict jet in wrong position and model shows higher velocity in peak. PIV measurement reported 0.88Vx/V, SBES prediction indicated 0.80Vx/V, while k-w SST 1.33Vx/V. Observed position of velocity peak is at 0.167y/Y, while CFD predictions shown it at 0.19y/Y for SBES and at 0.24y/Y for RANS k-w SST. Furthermore, velocity profile shape in SBES is parabolic, that is found to be similar to test results, while RANS based methods shown much more peaky shapes. Comparison on line L3 shows superiority of SBES based model, however comparison on planes located more downstream, near build plate where jet is attached to the bottom wall (Figure 8), do not show this advantage in SBES model. RANS approach predictions are quantitatively as close to the experiment and as SBES results. Maximum value reported in test is 1Vx/V SBES model and RANS RSM show 0.9Vx/V, while k-w SST 1.03Vx/V. There are also visible differences in curve slopes. SBES predicts lowest dVx/dy values from tested methods.

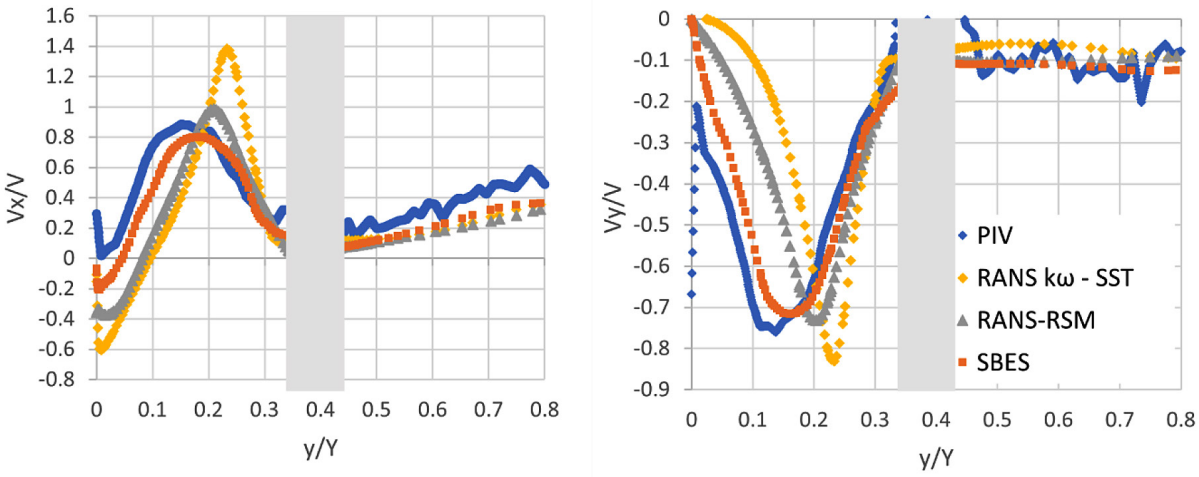

Figure 7. Methods comparison on line L3

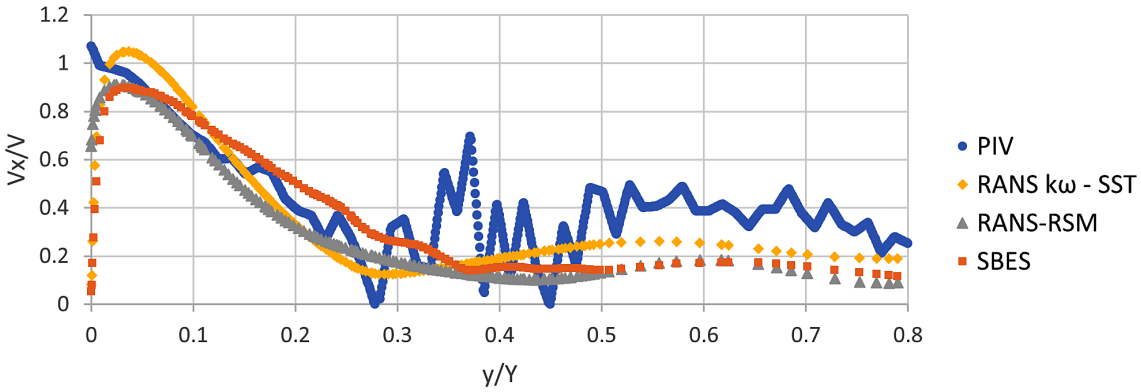

Figure 8. Methods comparison on line L9

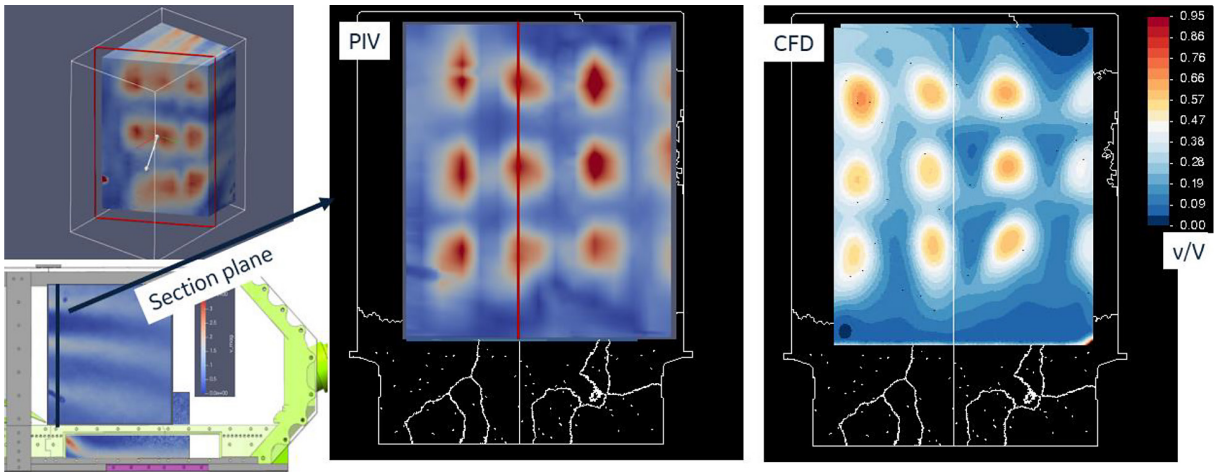

Figure 9. Upper flow velocity structure

Upper flow comparison between experiment and SBES CFD results show many similar velocity structure, but there are differences that, need to be pointed. In CFD model and in PIV measurement array of 4x3 jets is visible. Jets in the most on the right column in Figure 9 are the weakest. Entire flow structure observed on demonstrator is shifted to right that, second column is in the centerplne of chamber. Analytical results show jets positions less deflected, however position shift is also present. CFD predict lower velocities in jets. Value seen in analysis results is 0.57–0.71 of reference velocity value, while PIV measurement shows 0.95-1.14. That suggest, that CFD model predicts more dissipation on conditioning section flow structure, than it was present in the test. The same discrepancy has been observed for other two methods. It is believed, that these differencies are caused by lack of undestanding of how conditioning section behaves. Explenation will require additioinal investigation of flow field in conditioning section itself.

CONCLUSIONS

Presented work is focused on experimental and analytical investigations. Particle Image Velocimetry technique has been used to investigate inert gas flow. Measurements delivered qualitative and quantitative insight into DMLM printer chamber flow field. Data have been collected to understand flow behavior and gather quantitative flow field data for validation. Current case proved usefulness of PIV method for DMLM printer design. It delivered important information about flow structure that is difficult identify with typical anemometry. Test confirmed high quality purge flow structure venting printer chamber, as it was desired. Delivered results convince to involve PIV visualization technique into chamber redesign process and future printer design. Flow visualization revealed flow structures, that been observed before only with CFD modelling, that has some imperfections. In the other hand it is important to highlight, that PIV measurements consumed significant amount of work for preparation phase. Full scale model of printer chamber had to be designed and manufactured to enable optical access for laser and camera and maintain proper air supply conditions. This fact limits usefulness of this experimental method to usage at final proof of concept or cases, where design modifications can be easily implemented.

CFD calculations has been conducted to replicate the test. Conducted study delivered comprehensive information about CFD prediction quality and potential advantage of high fidelity (LES based) turbulence model usage. Three different turbulence models have been tested. Qualitatively all methods well reflected PIV measurements. Quantitative results analysis shown, that SBES method resolved lower flow jet with highest accuracy. Significant quantitative differences have been found in upper flow velocity structure. Reason of this discrepancy need further investigation and will be addressed in the future work.

Comprehensive research on gas flow in the printer's process chamber involving the use and correlation of the CFD analytical method with direct PIV measurement on the demonstrator of the LPBF printer's process chamber is an innovative idea enabling a more accurate and precise determination of flow phenomena occurring in the

3D printing process. The CFD results obtained so far were compared with point anemometric measurements, based on which only partial information about the conditions in the process chamber was obtained. The proposed methodology using PIV measurements allows for three-dimensional imaging of the actual state and relating it to the results of numerical analyses. In the future, such a methodology will be able to support the development of new designs of the printer process chamber and may also be used in the process of developing the parameters of new materials.

Acknowledgements

Work has been conducted within project RPMA.01.02.00-14-B479/18 funded by Regionalny Program Operacyjny Województwa Mazowieckiego.

REFERENCES

1. Cobbinah, P.V.; Nzeukou, R.A.; Onawale, O.T.; Matizamhuka, W.R. Laser Powder Bed Fusion of Potential Superalloys: A Review. Metals, 2021, 11, 58. http://doi.org/10.3390/met11010058
2. Kozak J., Zakrzewski T., Witt M., Dębowska-Wąsak, M., Selected Problems of Additive Manufacturing Using SLS/SLM Processes. Transactions on Aerospace Research, 1, 2021, 24–44.
3. Ladewig A., Schlick G., Fisser M., Schulze V., Glatzel U., Influence of the shielding gas flow on the removal of process by-products in the selective laser melting process. Additive Manufacturing, 10, 2016, 1-9.
4. Reijonen J., Revuelta A., Ruusuvuori K., Puukko P., On the effect of shielding gas flow on porosity and melt pool geometry in laser powder bed fusion additive manufacturing. Additive Manufacturing, 32, 2020, 101030.
5. Ferrar B., Mullen L., Jones E., Stamp R., Sutcliffe C. J. Gas flow effects on selective laser melting (SLM) manufacturing performance. Journal of Materials Processing Technology, 212(2), 2012, 355-364.
6. Nadimpalli P., Christiansen T., Andersen S., Kjer M., Mishin O., Zhang Y., Influence of shielding gas flow on the uniformity of additively manufactured martensitic stainless steel, IOP Conf. Series: Materials Science and Engineering, 2022.
7. Anwar A., Pham Q., Effect of inert gas flow velocity and unidirectional scanning on the formation and accumulation of spattered powder during selective laser melting. Proc. of the 2nd Intl. Conf. on Progress in Additive Manufacturing, 2016.
8. Shen H., Rometsch P., Wu X., Huang A., Influence of gas flow speed on laser plume attenuation and powder bed particle pickup in laser powder bed fusion. JOM, 72(3), 2020.
9. Roidl B., Fauner T., Continuous Improvement in Gas Flow Design. Whitepaper, https://go.additive.ge.com/rs/706-JIU-273/images/GE%20Additive_Gas%20Flow_WP_US_EN-high%20res.pdf, GE Additive, 2022.
10. Philo A., Sutcliffe C., Sillars S., Sienz J., Brown S., Lavery N., Study into the effects of gas flow inlet design of the renishaw Am250 laser powder bed fusion machine using computational modelling. Solid Freeform Fabrication 2017: Proceedings of the 28th Annual International Solid Freeform Fabrication Symposium – An Additive Manufacturing Conference, 1203-1219.
11. Philo A., Lavery N., Brown S., Cherry J., Sienz J., Joannou J., Sutcliffe C., Comparison and validation of gas flow models in a powder bed selective laser melting process. In: Proc. of the 23rd UK Conference of the Association for Computational Mechanics in Engineering, 2015, 189-195.
12. Chen Y., Vastola G., Zhang Y., Optimization of inert gas flow inside laser powder bed fusion chamber with computational fluid dynamics. In: Proc.of the 29th Annual International Solid Freeform Fabrication Symposium – An Additive Manufacturing Conference. Solid Freeform Fabrication, 2018.
13. Weaver J., Schlenoff A., Deisenroth D., Moylan S., Inert gas flow speed measurements in laser powder bed fusion additive manufacturing. Advanced Manufacturing Series, 2021.
14. Chen X., Wang W., The applications of particle image velocimetry (PIV) to experimentally observe the flow behaviors inside the selective laser melting (SLM) working chamber. Flow Measurement and Instrumentation, 73, 2020: 101738.
15. Schniedenharn M., Wiedemann F., Schleifenbaum J., Visualization of the shielding gas flow in SLM machines by space-resolved thermal anemometry. Rapid Prototyping Journal, 24/8, 2018: 1296–1304.
16. Chen X., Tzeng S., Wang W., Numerical and experimental observations of the flow field inside a selective laser melting (SLM) chamber through computational fluid dynamics (CFD) and particle image velocimetry (PIV). Powder Technology, 362, 2020, 450-461,
17. Chien C., Le T., Lin Z., Lo Y., Numerical and experimental investigation into gas flow field and spattering phenomena in laser powder bed fusion processing of Inconel 718. Materials & Design, 210, 2021, 110-107.
18. Elsinga G.E., Scarano F., Wieneke B., van Oudheusden B.W., Tomographic particle image velocimetry. In: 6th Int. Symp. Part. Image Velocim.,

1–12, 2005. Available: http://www.springerlink.com/index/17008530406263N2.pdf.

19. Kähler C.J. and Kompenhans J., Fundamentals of multiple plane stereo particle image velocimetry. Exp. Fluids, 29(7), S070–S077, 2000, doi: 10.1007/s003480070009.
20. Scarano F., Tomographic PIV: Principles and practice. Meas. Sci. Technol., vol. 24, no. 1, 2013, doi: 10.1088/0957-0233/24/1/012001.
21. Czyż Z., Karpiński P., Stryczniewicz W., Measurement of the flow field generated by multicopter propellers. Sensors (Switzerland), 20(19), 2020,1–22, doi: 10.3390/s20195537.
22. Czyż Z. and Stryczniewicz W., Investigation of aerodynamic interference in a multirotor by PIV method. Adv. Sci. Technol. Res. J., 12(1), 2018, 106–114, doi: 10.12913/22998624/86475.
23. Laskin S., Submerged aerosol unit. AEC Project Quarterly Report UR-38, 1948.
24. Raffel M. et al., Particle Image Velocimetry: A Practical Guide. Springer, 2007.
25. Theunissen R., Scarano F., Riethmuller M., An adaptive sampling and windowing interrogation method in PIV. Meas. Sci. Technol., 18, 2007, 275–287.
26. Frant M., Kozakiewicz A., Kachel S., Analysis of impact of gust angle and velocity on the position of stagnation point. Adv. Sci. Technol. Res. J. 2020; 14(4): 49–57.
27. Ansorge R., Mathematical Models of Fluid Dynamics. Willey-VCH GmbH &Co. 2003.
28. Cokljat D., Caradi D., Link G., Lechner R., Menter F., Embedded LES methodology for general-purpose CFD solvers. In: Proc. 6th Int. Symp. Turbulence and Shear Flow Phenomena, 2009, 1191-1196.